MEMBRANES

Zeolitic imidazolate framework membranes made by ligand-induced permselectivation

Xiaoli Ma*†, Prashant Kumar†, Nitish Mittal†, Alexandra Khlyustova, Prodromos Daoutidis, K. Andre Mkhoyan, Michael Tsapatsis*

Zeolitic imidazolate framework (ZIF) membranes are emerging as a promising energy-efficient separation technology. However, their reliable and scalable manufacturing remains a challenge. We demonstrate the fabrication of ZIF nanocomposite membranes by means of an all-vapor-phase processing method based on atomic layer deposition (ALD) of ZnO in a porous support followed by ligand-vapor treatment. After ALD, the obtained nanocomposite exhibits low flux and is not selective, whereas after ligand-vapor (2-methylimidazole) treatment, it is partially transformed to ZIF and shows stable performance with high mixture separation factor for propylene over propane (an energy-intensive high-volume separation) and high propylene flux. Membrane synthesis through ligand-induced permselectivation of a nonselective and impermeable deposit is shown to be simple and highly reproducible and holds promise for scalability.

Substantial energy and capital cost savings are possible by using membrane-based separations (*1*). Among the membrane materials that have been explored, zeolitic imidazolate frameworks (ZIFs) (*2*, *3*), particularly ZIF-8 and ZIF-67 (*4*–*6*), exhibit promising performance for the processing of important industrial mixtures, such as propylene/propane (*7*), that are considered challenging to separate efficiently with the currently used distillation-based methods (*8*, *9*). ZIF-8 membranes have been fabricated as continuous thin films on the outer surface or inside porous ceramic (*10*–*12*) or polymeric supports (*13*, *14*) with solution-based methods that are difficult to scale up. Replacing all solvothermal steps with completely solvent-free processing has environmental, cost, and scale-up advantages and has been adapted successfully for seeded growth of zeolite membranes (*15*, *16*). Recently, an all-vapor deposition technique was reported for the fabrication of metal-organic framework (MOF) thin films on silicon wafers for microelectronic applications (*17*). It is based on a combination of oxide deposition by means of atomic layer deposition (ALD), followed by 2-methylimidazole (mIm) ligand-vapor treatment to convert the ALD-deposited oxide to ZIF. However, only aspects of this approach have been adapted for membrane preparation, and an all-vapor membrane synthesis method is yet to be demonstrated (*18*, *19*). Here, we report the liquid/gel-free and seed-free synthesis of high-performance membranes through ligand-induced permselectivation (LIPS) of a nonselective and impermeable deposit (Fig. 1A). Distinct from all prior methods that aim to create a thin selective MOF molecular sieve layer by gradually filling the pores of a support or by forming a deposit on its surface, the current method first blocks the pores with an impermeable deposit, which is then transformed by means of LIPS to a selective MOF. As a result, the inherent drawback associated with all pore-filling membrane growth methods, which leave behind nonselective transport pathways (such as pinholes and nonselective grain boundaries), is circumvented.

α-Alumina macroporous substrates coated with a ~5-μm γ-alumina mesoporous layer with pores in the 2 to 5 nm range (*20*) were used as the supports. They can be made easily based on well-known procedures and are amenable to scale up in disc or tubular geometries. They have propylene permeance of 10^{-6} mol Pa^{-1} m^{-2} s^{-1} and do not exhibit propylene/propane selectivity. During ALD, diethylzinc reacts with the surface hydroxyl groups that are present in the mesopores of the γ-alumina layer. Subsequent introduction of water vapor yields hydroxylated zinc oxide, completing an ALD cycle. This process is repeated for up to 50 cycles so as to obtain a zinc oxide and/or zinc hydroxide (called ZnO from now on) deposit on top and inside the γ-alumina layer. As shown by the open symbols in Fig. 1B, an initially gradual propylene permeance reduction is followed by a large drop after 10 ALD cycles of ZnO. Specifically, for up to eight ALD cycles, propylene permeance remained above 10^{-8} mol Pa^{-1} m^{-2} s^{-1}, whereas after 10 ALD cycles, the resulting ZnO-alumina composite is rendered essentially impermeable, with a propylene permeance falling by more than four orders of magnitude to 2×10^{-11} mol Pa^{-1} m^{-2} s^{-1}, indicating that the pores of the substrate are essentially blocked for propylene by the ALD deposit. The abrupt permeance drop is typical of percolation-based densification observed in dense membranes formed through chemical vapor deposition of oxides inside porous supports (*21*, *22*). At no point during ALD do the membranes exhibit propylene/propane selectivity (Fig. 1C, open triangles).

After exposing the impermeable and nonselective 10-cycle ALD–modified supports to vapors generated by the sublimation of mIm, propylene permeance and propylene/propane selectivity increase by three and two orders of magnitude, respectively, as indicated by the tie-lines with the upward pointing arrows in Fig. 1, B and C. ZnO deposits of more than 20 cycles result in membranes with lower permeance (Fig. 1B). Membranes obtained from ZnO made by less than 10 ALD cycles showed relatively low selectivity (5 to 20) and higher permeances of ~10^{-7} mol Pa^{-1} m^{-2} s^{-1} (Fig. 1, B and C). Although these higher-flux lower-selectivity membranes could be of interest, here we focus on 10 and 20 cycles of ALD that reproducibly yield membranes with high selectivity (~100) and good permeance (>10^{-8} mol Pa^{-1} m^{-2} s^{-1}). Because of the ligand-induced transformation from an impermeable to selective membrane, the process described here is named LIPS.

The overall performances of LIPS membranes, in terms of propylene permeance and propylene/propane selectivity, are among the best that have been reported for both ZIF-8 and ZIF-67 membranes (Fig. 1D and table S1) (*5*, *6*, *10*, *13*, *18*, *19*, *23*–*28*). Under an equimolar propylene/propane mixture feed, and pressure as high as ~7 atm, the membranes made by means of LIPS exhibit a combination of high selectivity/separation factor and high propylene flux (Fig. 1E). In addition, stable performance in mixed gas separation tests under a feed pressure from 1 to 7 atm was demonstrated (fig. S1). Moreover, heating the membrane under equimolar 1 atm propylene/propane feed to 60°C for ~36 hours did not alter the room-temperature membrane performance. At 7 atm feed, depending on feed composition and permeate conditions (vacuum and 1 atm undiluted permeate), typical propylene fluxes range from 0.01 to 0.06 mol m^{-2} s^{-1} with separation factors of ~50 to 70 (figs. S2 and S3). A conservative process-scale assessment (*29*) shows promise for large-scale uses such as de-bottlenecking of distillation columns in order to increase processing capacity.

To illuminate the membrane microstructure, reveal the location of the ZIF-8–selective layer, and relate it with that of the as-made and ALD-modified alumina support, we used x-ray diffraction (XRD) and electron microscopy imaging, coupled with gradual ZIF-8 removal through water washing. A high-angle annular dark-field scanning transmission electron microscopy (HAADF-STEM) image of a cross section of the porous support (γ-alumina supported on α-alumina) prepared by focused ion beam is shown in Fig. 2A along with Al and Zn spatial maps obtained with energy-dispersive x-ray (EDX) spectral imaging and the corresponding Al- and Zn-composition line scans. As expected, the support does not contain any Zn. The 5-μm uniform γ-alumina mesoporous layer is clearly distinguished from

Department of Chemical Engineering and Materials Science, University of Minnesota, 421 Washington Avenue SE, Minneapolis, MN 55455, USA.
***Corresponding author. Email: tsapatsis@umn.edu (M.T.); maxx0183@umn.edu (X.M.)** †These authors contributed equally to this work.

the underlying α-alumina macroporous support. The corresponding images and scans after 10 cycles of ALD (before mIm-vapor treatment) are shown in Fig. 2B. Zn is detected throughout the γ-alumina layer but is mostly present at its top 200 nm. There is no detectable Zn in the α-alumina. The line scans in Fig. 2B indicate that Zn is also present as a thin layer on the outside surface of the γ-alumina layer. Top-view scanning electron microscopy (SEM) imaging shows the presence of partially intergrown nanoparticles, which have distinct morphology compared with that of the fibrous appearance of the γ-alumina top surface (fig. S4, A and B) and can be attributed to ZnO that was deposited outside the pores of the support. The drastic reduction in propylene permeance, which essentially renders the membrane propylene-impermeable after 10 ALD cycles (Fig. 1), can be attributed to γ-alumina mesopore blockage by this thin (less than 0.5 μm) deposit that is partly confined in the mesopores and partly present on their external top surface. The corresponding set after mIm-vapor-treatment is shown in Fig. 2C; the Zn distribution changes substantially. More Zn is now present within the rest of the γ-alumina layer, and a new Zn-containing deposit at the γ-alumina/α-alumina interface is evident. The observations described above are more clearly visible in Fig. 2, D to F, which shows the corresponding higher-magnification cross-sectional images from the top and bottom parts of the γ-alumina before (Fig. 2D) and after ALD (Fig. 2E) and after mIm-vapor treatment (Fig. 2F).

The altered Zn profiles demonstrate that during mIm-vapor treatment, the ALD-deposited Zn can be mobilized and transported by diffusion throughout the 5-μm γ-alumina mesoporous layer. Consistently, nitrogen-composition line-scans indicate the presence of mIm throughout the γ-alumina layer, with higher concentrations at the top and bottom (fig. S5), which is coincident with the Zn content maxima. The pronounced redistribution of the deposited Zn suggests formation of Zn-mIm species with increased surface mobility compared with that of the ALD-deposited ZnO. In the geometry used for mIm-vapor treatment, mIm vapors are introduced from both sides of the γ-alumina layer (not only from its top side but also from the bottom γ-alumina/α-alumina interface), reacting with and mobilizing the deposited ZnO in the interior of the γ-alumina layer. The earlier report on mIm-vapor treatment of the ALD-deposited ZnO is also suggestive of Zn-mIm mobile species because the morphology of the ZIF-8 crystals formed upon exposure to mIm is coarsened with respect to that of the ALD-deposited oxide (*17*).

Considering the low ZIF density, if we assume full conversion to ZIF-8, the levels of Zn detected within the γ-alumina layer after mIm-vapor treatment are sufficient to fill the 2- to 5-nm pores and create a selective ZIF deposit. However, the high levels of Zn remaining near, and at the top, of the γ-alumina layer indicate that not all of the ALD-deposited ZnO has been transformed to ZIF after mIm-vapor treatment (there should be a substantial remaining unconverted ZnO fraction). This is further corroborated with

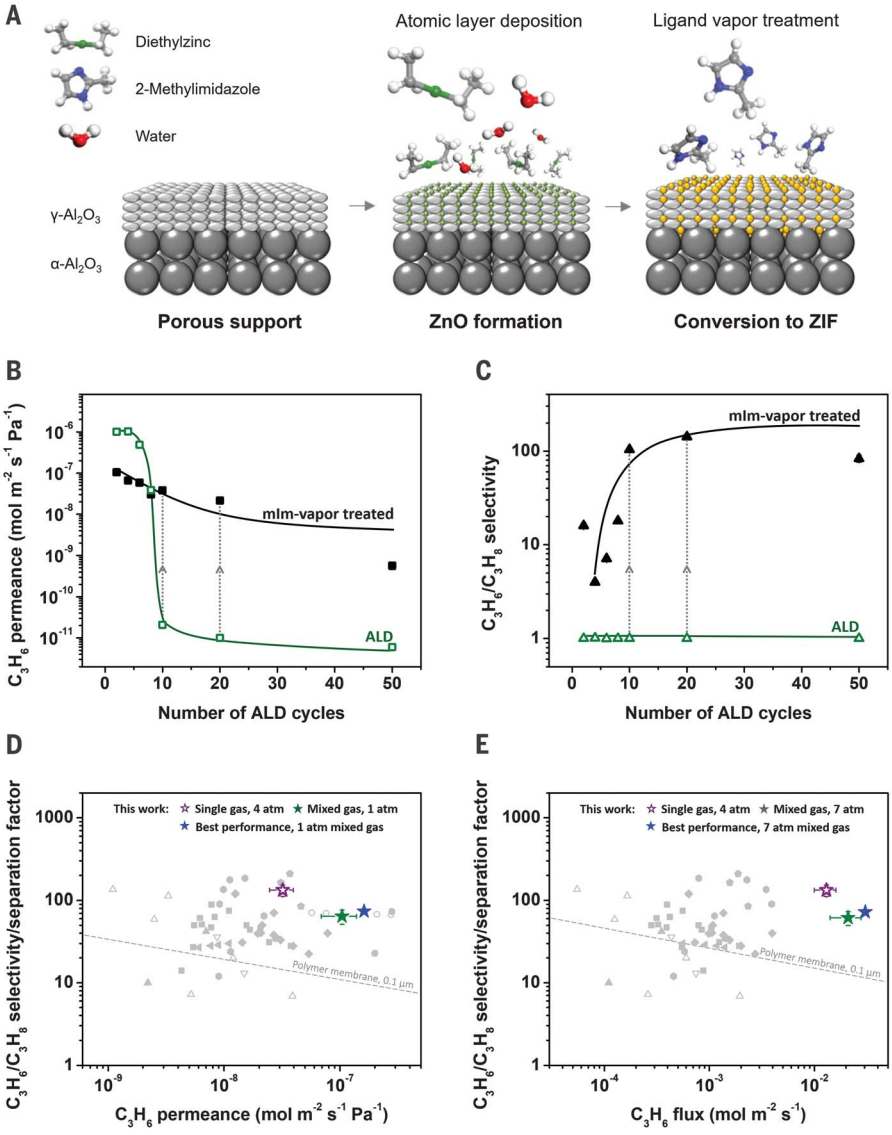

Fig. 1. Permeation properties of membranes made by LIPS. (**A**) Schematic of the all-vapor-phase LIPS membrane fabrication process. The pores of support are first blocked with ZnO made by means of ALD. The impermeable ZnO deposits are converted to ZIF by means of ligand-vapor treatment. (**B** and **C**) Propylene permeances (B) and propylene/propane single-component selectivities (C) of the ZIF-8/γ-alumina nanocomposite membranes as a function of the number of ALD cycles (solid symbols). Open symbols are values obtained from a support treated by the indicated cycles of ZnO ALD (before the ligand-vapor treatment). The tie lines connect them with the corresponding values obtained after the ligand-vapor treatment. (**D** and **E**) Propylene/propane single-component selectivities (open symbols) and equimolar mixture separation factors (solid symbols) versus propylene permeance (D) and versus propylene flux (E) obtained from the ZIF-8/γ-alumina nanocomposite membranes and as reported in the literature [solid square, (*5*, *23*); left-pointing solid triangle, (*24*);up-pointing open triangle, (*25*); up-pointing solid triangle, (*26*); down-pointing open triangle, (*27*); solid pentagon, (*6*); solid diamond, (*10*, *18*); solid circle, (*19*); solid hexagon, (*13*, *28*); and additional references cited in table S1]. The feed pressure for single-component permeation test is ~4 atm, and the feed pressure for mixed gas (equimolar feed) separation test is 1 atm in (D) and ~7 atm in (E). The performance data are the average values of six different nanocomposite membranes made from 10 and 20 cycles ZnO ALD. The lines represent Robeson upper bounds for polymeric membranes (*32*) assuming polymer thickness of 0.1 μm and, for the estimation of flux in (E), a 7-atm equimolar feed.

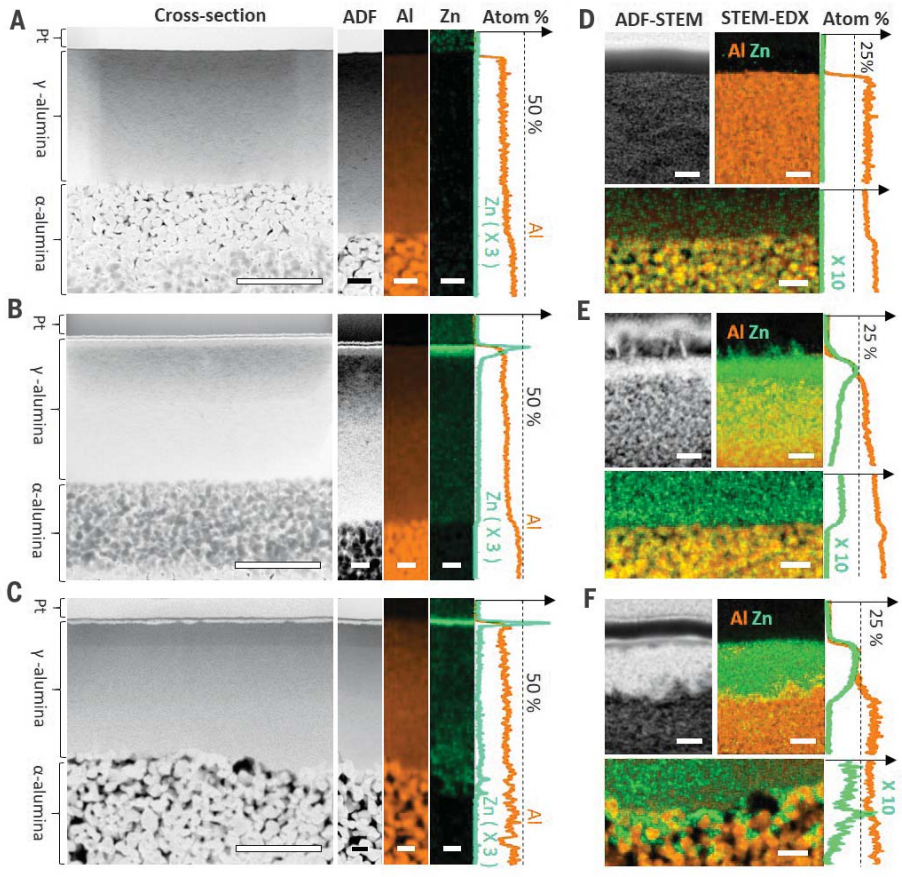

Fig. 2. Microstructure of membranes made by means of LIPS. (**A** to **C**) Cross section analysis with ADF-STEM imaging, corresponding spatial distribution of aluminum (orange) and zinc (green), and the averaged atomic percentage across the same section along the depth for (A) γ-alumina on α-alumina support, (B) after ZnO deposition by ALD, and (C) after mIm ligand-vapor treatment. Zinc atomic percentage has been magnified three times for clarity. (**D** to **F**) Magnified views of top (γ-Al_2O_3) and bottom (γ-Al_2O_3/α-Al_2O_3 interface) sections of (A) to (C), respectively. Zinc signal has been amplified 10 times for the γ-Al_2O_3/α-Al_2O_3 section for visibility. (A) to (C), large scale bars, 2 μm; small scale bars, 400 nm. (D) to (F), small scale bars (top), 50 nm; larger scale bars (bottom), 500 nm.

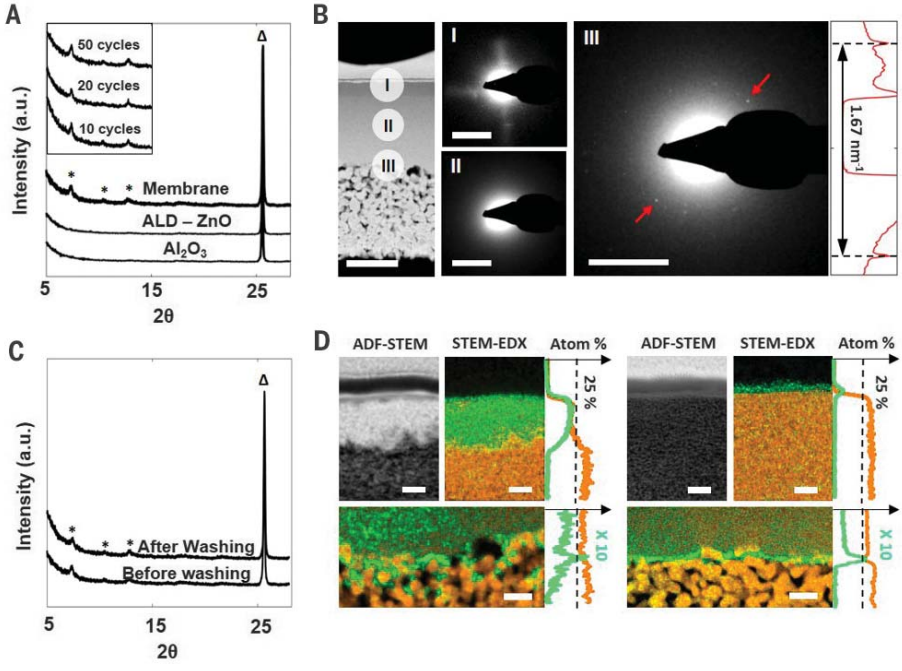

Fig. 3. Diffraction analysis of LIPS membranes before and after partial deposit removal by water washing. (**A**) XRD patterns of alumina support (5-μm-thick γ-alumina supported on α-alumina), of the nanocomposite obtained after 10 cycles of ZnO ALD, and of the ZIF-8/γ-alumina nanocomposite membrane obtained after ligand-vapor treatment of the ZnO deposit made with 10 ALD cycles. (Inset) Magnified views of the XRD patterns (2θ range of ZIF-8) of membranes prepared after ligand-vapor treatment of the ZnO deposit made by 10, 20, and 50 ALD cycles. Asterisks and open triangles indicate ZIF-8 and α-alumina peaks, respectively. (**B**) Selected area ED patterns acquired at different depths as marked in the cross section. Diffraction patterns I and II show no evidence of crystallinity, whereas pattern III shows sharp spots. Line scans across the spots indicated with red arrows show interplanar distances of 1.2 nm (0.83 nm^{-1}) corresponding to (011) spacing for ZIF-8 structure. Scale bars, 1 nm^{-1}. (**C**) Diffraction patterns acquired from a ZIF membrane before and after washing. Asterisks and open triangles indicate ZIF-8 and α-alumina peaks, respectively. (**D**) ADF-STEM image and the corresponding spatial elemental distribution of aluminum (orange) and zinc (green) in (top) γ-Al_2O_3 and (bottom) γ-Al_2O_3/α-Al_2O_3 interface of (left) ZIF membrane before washing and (right) ZIF membrane after washing. The zinc signal has been amplified 10 times for the γ-Al_2O_3/α-Al_2O_3 section for visibility. Scale bars, top, 50 nm; bottom, 500 nm.

top-view SEM imaging (fig. S4C) that shows preservation of the nanoparticulate microstructure with enlarged grain appearance that can be attributed to, at most, a partial transformation of the ALD deposit to ZIF.

We attempted to detect the presence of ZIF-8 with XRD and electron diffraction (ED). After imidazole-vapor treatment, XRD peaks that are characteristic of ZIF-8 can be clearly detected (Fig. 3A). Examination of the membrane cross section by means of ED (Fig. 3B) shows that ZIF-8 is detectable only at the γ-alumina/α-alumina interface. In the other regions of the γ-alumina layer, crystalline ZIF-8 could not be detected despite the presence of Zn. This finding raised the question of whether the deposit at the γ-alumina/α-alumina interface is solely responsible for the selective membrane performance.

To answer this question, the γ-alumina top side of a membrane was washed with flowing deionized (DI) water in order to gradually dissolve the ZIF-8 or ZIF-8–like deposits and alter its permeation performance and microstructure. In a control experiment, it was determined that washing with water, a 10-ALD-cycle membrane (before imidazole-vapor treatment) did not alter its characteristic, propylene-impermeable performance. By contrast, the permeation performance of the ZIF-8 membrane changed upon washing. After a first washing with 100 g of DI water, the propylene permeance of the membrane tested increased from 170 to 195 gas permeation units (GPU), while the mixture separation factor decreased from 45 to 5.6. After a second washing, the propylene permeance increased to 329 GPU, and the separation factor dropped to 1.7. XRD of the membrane after the second washing did not reveal substantial changes in the ZIF-8 reflections (Fig. 3C). By contrast, cross-sectional examination by means of HAADF-STEM and spectral imaging (Fig. 3D) revealed that the Zn present within the γ-alumina layer decreased, whereas the ZIF-8 present at the γ-alumina/α-alumina interface was largely preserved.

These results reveal that the deposit in the γ-alumina/α-alumina interface is the major contributor to the detectable XRD ZIF-8 reflections, but the propylene-selective performance of the membrane is mostly due to the deposit within and on top of the γ-alumina layer. The lack of detectable crystallinity in the selective layer may be attributed to its confinement within the small 2- to 5-nm pores of the γ-alumina layer and in between the ZnO grains of the top deposit. The high separation factors achieved should then be attributed mostly to this not well-crystallized ZIF deposit and could be explained by the recently identified structural similarities of ZIF-8 and amorphous ZIFs (*30*, *31*).

The LIPS process, demonstrated here, establishes a reliable, scalable, and robust approach for the fabrication of ZIF and possibly other MOF membranes and nanocomposites. Unlike other molecular sieve membrane fabrication methods, which rely on solvothermal nucleation and growth that is difficult to reliably scale up, the method shown here is based on scalable, solvent-free, seed-free, all-vapor processing with ALD, a well-established materials processing technology.

REFERENCES AND NOTES

1. D. S. Sholl, R. P. Lively, *Nature* **532**, 435–437 (2016).
2. K. S. Park *et al.*, *Proc. Natl. Acad. Sci. U.S.A.* **103**, 10186–10191 (2006).
3. H. Furukawa, K. E. Cordova, M. O'Keeffe, O. M. Yaghi, *Science* **341**, 1230444 (2013).
4. H. Bux *et al.*, *J. Am. Chem. Soc.* **131**, 16000–16001 (2009).
5. Y. C. Pan, T. Li, G. Lestari, Z. P. Lai, *J. Membr. Sci.* **390-391**, 93–98 (2012).
6. H. T. Kwon, H. K. Jeong, A. S. Lee, H. S. An, J. S. Lee, *J. Am. Chem. Soc.* **137**, 12304–12311 (2015).
7. K. Li *et al.*, *J. Am. Chem. Soc.* **131**, 10368–10369 (2009).
8. R. B. Eldridge, *Ind. Eng. Chem. Res.* **32**, 2208–2212 (1993).
9. M. Galizia *et al.*, *Macromolecules* **50**, 7809–7843 (2017).
10. M. J. Lee, H. T. Kwon, H. K. Jeong, *Angew. Chem. Int. Ed.* **57**, 156–161 (2018).
11. E. Jang *et al.*, *J. Membr. Sci.* **540**, 430–439 (2017).
12. M. Drobek *et al.*, *J. Membr. Sci.* **475**, 39–46 (2015).
13. A. J. Brown *et al.*, *Science* **345**, 72–75 (2014).
14. S. C. Hess, R. N. Grass, W. J. Stark, *Chem. Mater.* **28**, 7638–7644 (2016).
15. T. C. T. Pham, T. H. Nguyen, K. B. Yoon, *Angew. Chem. Int. Ed.* **52**, 8693–8698 (2013).
16. M. Y. Jeon *et al.*, *Nature* **543**, 690–694 (2017).
17. I. Stassen *et al.*, *Nat. Mater.* **15**, 304–310 (2016).
18. H. T. Kwon *et al.*, *Chem. Commun.* **52**, 11669–11672 (2016).
19. W. Li *et al.*, *Nat. Commun.* **8**, 406 (2017).
20. C. H. Chang, R. Gopalan, Y. S. Lin, *J. Membr. Sci.* **91**, 27–45 (1994).
21. Y. S. Lin, A. J. Burggraaf, *Chem. Eng. Sci.* **46**, 3067–3080 (1991).
22. M. Tsapatsis, G. R. Gavalas, *AIChE J.* **38**, 847–856 (1992).
23. Y. C. Pan, W. Liu, Y. J. Zhao, C. Q. Wang, Z. P. Lai, *J. Membr. Sci.* **493**, 88–96 (2015).
24. D. F. Liu, X. L. Ma, H. X. Xi, Y. S. Lin, *J. Membr. Sci.* **451**, 85–93 (2014).
25. N. Hara *et al.*, *J. Membr. Sci.* **450**, 215–223 (2014).
26. N. Hara *et al.*, *J. Jpn. Petrol. Inst.* **58**, 237–244 (2015).
27. S. Tanaka, K. Okubo, K. Kida, M. Sugita, T. Takewaki, *J. Membr. Sci.* **544**, 306–311 (2017).
28. K. Eum *et al.*, *Adv. Funct. Mater.* **26**, 5011–5018 (2016).
29. Materials and methods are available as supplementary materials.
30. P. Adhikari *et al.*, *J. Phys. Chem. C* **120**, 15362–15368 (2016).
31. H. Tao, T. D. Bennett, Y. Yue, *Adv. Mater.* **29**, 1601705 (2017).
32. W. J. Koros, R. P. Lively, *AIChE J.* **58**, 2624–2633 (2012).

ACKNOWLEDGMENTS

The authors acknowledge R. Agrawal and his group (Purdue University) for a valuable discussion. **Funding:** This work was supported by the Center for Gas Separations Relevant to Clean Energy Technologies, an Energy Frontier Research Center funded by the U.S. Department of Energy, Office of Science, Basic Energy Sciences under award DE-SC0001015. Parts of this work were carried out in the Characterization Facility, University of Minnesota and the Minnesota Nano Center, which receive partial support from the National Science Foundation through the Materials Research Science and Engineering Center and National Nanotechnology Coordinated Infrastructure programs, respectively. SEM measurements were partially performed on a Hitachi 8230 provided by NSF MRI DMR-1229263. **Author contributions:** M.T. and X.M. conceived the project. X.M. and A.K. prepared the supports. X.M. prepared and tested the membranes. X.M. performed permeation testing, XRD, and SEM. P.K. performed STEM and EDX imaging and analyzed the data with input from M.T. and K.A.M. N.M. performed the process-scale assessment with input from M.T. and P.D. M.T. directed all aspects of the project. M.T., X.M., P.K., and N.M. wrote the manuscript with input from all coauthors. **Competing interests:** The authors declare no competing interests. **Data and materials availability:** All data are available in the manuscript or the supplementary materials.

SUPPLEMENTARY MATERIALS

www.sciencemag.org/content/361/6406/1008/suppl/DC1
Materials and Methods
Supplementary Text
Figs. S1 to S10
Tables S1 and S2
References (*33*–*73*)

25 February 2018; accepted 6 July 2018
10.1126/science.aat4123

Science

Zeolitic imidazolate framework membranes made by ligand-induced permselectivation

Xiaoli Ma, Prashant Kumar, Nitish Mittal, Alexandra Khlyustova, Prodromos Daoutidis, K. Andre Mkhoyan and Michael Tsapatsis

Science **361** (6406), 1008-1011.
DOI: 10.1126/science.aat4123

The makings of permeable membranes

A challenge in making membranes is finding ways to control the pore structure during the fabrication process or through postfabrication treatment. The deposition of a zeolitic imidazolate framework material called ZIF-8 onto an alumina support gives a dense, impermeable material. However, when Ma *et al.* exposed this material to vapors of 2-methylimidazole, it transformed into a porous material able to separate propylene from propane.

Science, this issue p. 1008